

# Analysis and Design of a Dual-Rotor Axial-Flux Vernier Permanent Magnet Machine

Tianjie Zou, *Student Member, IEEE*, Ronghai Qu, *Senior Member, IEEE*, Jian Li, *Member, IEEE*, and Dawei Li, *Student Member, IEEE*,  
State Key Laboratory of Advanced Electromagnetic Engineering and Technology  
School of Electrical & Electronic Engineering  
Huazhong University of Science and Technology, Wuhan, 430074, China  
E-mail:ronghaiqu@mail.hust.edu.cn

**Abstract**—This paper proposes a dual-rotor, toroidal-winding, axial-flux vernier permanent magnet (VPM) machine. By the combination of toroidal windings with the rotor-stator-rotor topology, the end winding length of the machine is significantly reduced when compared with the regular VPM machine. Based on the airgap permeance function, the back-EMF and torque expressions are derived, through which the nature of this machine is revealed. The influence of pole ratio (ratio of rotor pole pair number to stator pole pair number) and main geometric parameters such as slot opening, magnet thickness etc., on torque performance is then analytically investigated. Both the quasi-3-dimensional (quasi-3D) finite element analysis (FEA) and 3D FEA are applied to verify the theoretical analysis. With the current density of 4.2 A/mm<sup>2</sup>, the torque density of the proposed machine can reach 32.6 kNm/m<sup>3</sup>. A prototype has been designed and is in manufacturing process. Experimental validation will be presented in the future.

**Index Terms**—Dual-rotor, toroidal-winding, axial flux, vernier machine, torque equation, quasi-3D FEA.

## I. INTRODUCTION

With the merits of high torque density and compact mechanical structure, vernier permanent magnet (VPM) machines are attracting more and more attentions [1-4]. Due to the so-called magnetic gearing effect [1], the rotor of a VPM machine rotates at a much slower speed than that of the stator magnetic field, which makes this kind of machine a suitable alternative for low-speed, high-torque applications such as wind power and ship propulsion.

Many researches about VPM machines focused on proposing novel machine topologies [5-8]. General back-EMF and torque equations of radial flux VPM machines were derived in [9][10] to investigate the operation principles of VPM machines analytically.

Despite the strength in torque density, regular VPM machines tend to suffer long end windings, which results in larger machine size, as well as extra cost in heat dissipation. [7] proposed a dual-rotor VPM machine with short end winding length, in which toroidal windings were applied to take advantage of its dual airgap structure. [8] adopted concentrated windings on a special shaped stator with auxiliary teeth to shorten the end windings.

So far, most researches of VPM machine topologies are conducted on radial flux VPM machines. While in recent years, axial flux permanent magnet (AFPM) machines have become an important alternative to radial flux PM machines [11][12]. With the merits of high torque density, high efficiency and structure compactness, AFPM machines are becoming an attractive solution for certain applications where a large machine aspect ratio is required [13][14]. In recent years, A few topologies of axial flux VPM (AFVPM) machines have been proposed [15-17]. [15] deals with a dual stator, axial flux, spoke type VPM machine which has a high torque density as well as high power factor. In [16] a five-disk axial-flux-modulated machine is compared with its radial flux counterpart, which shares the same modulation effect with VPM machines. So far, neither the analytical back-EMF and torque expressions based on geometric parameters of AFVPM machines, nor deep analysis of parameters' effect upon these equations has been found in literature.

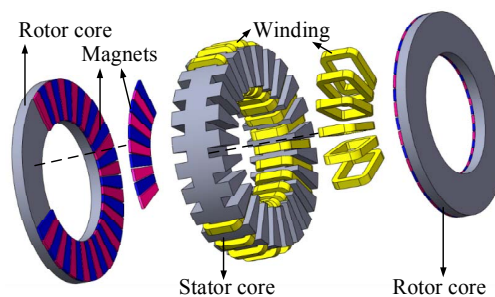


Fig. 1. Exploded view of the proposed AFVPM machine.

In this paper, a dual-rotor, toroidal-winding AFVPM machine is proposed as illustrated in Fig. 1, which combines the advantages of AFPM and VPM machines. Compared with regular VPM machines, this machine topology has advantages in end winding length. In Section II, the machine structure and operation principle will be introduced. Section III will be devoted to the back-EMF and torque derivation of the proposed machine. Some design parameters, such as slot opening, diameter ratio (ratio of inner to outer diameter), magnet thickness etc., will be investigated based on the analytical equations. Quasi-3-dimensional (quasi-3D) finite element analysis (FEA) [13] and 3D FEA will be used to verify the

theoretical analysis in Section IV. Finally, a prototype with optimized geometric parameters is designed and the auxiliary mechanical schematic will be introduced in Section V. The prototype is being manufactured and experimental validation is in plan.

## II. MACHINE STRUCTURE AND OPERATION PRINCIPLE

The exploded sketch of the proposed dual rotor AFVPM machine is shown in Fig. 1. Briefly, the proposed machine is constructed in a similar way with conventional dual rotor AFPM machine, including two rotors and one stator sandwiched between them. The surface mounted PMs on the two rotor disks are circumferentially aligned with each other and of opposite polarities, forming a North-North (NN) type TORUS topology [12]. Benefited from the rotor-stator-rotor structure combined with the NN type magnet polarity arrangement, toroidal windings can be used to significantly shorten the end winding length.

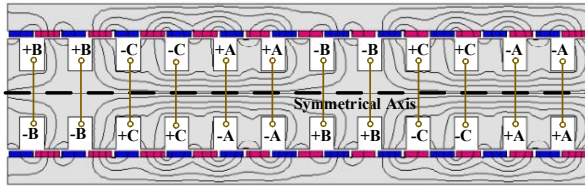


Fig. 2. Flux distribution along half the cylindrical surface of the proposed machine.

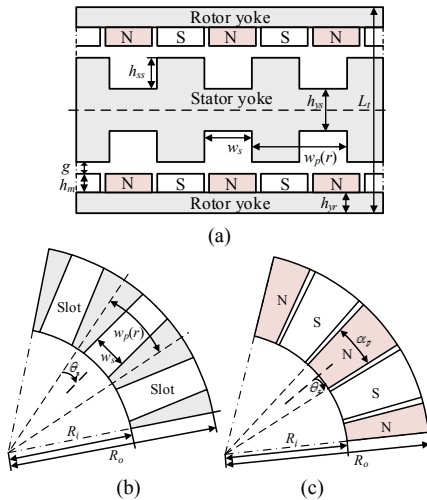


Fig. 3. Sketch of the proposed AFVPM machine with main geometric parameters. (a)cylindrical view. (b)top view of the stator. (c)top view of the rotor.

Fig. 2 illustrates the flux distribution along cylindrical surface of the proposed machine. Two strands of flux lines, driven by PMs on different rotors respectively, pass through two axial airgaps into the stator core and then travels circumferentially in the stator back iron. It can be clearly seen that the flux lines exhibit the property of mirror symmetry. Therefore, the design process can be simplified by focusing on only one rotor and half the stator. In comparison, the rotor-stator-rotor topology applied in radial flux VPM

machines will lead to a more complex design process, since the inner and outer rotors should be designed individually, as well as the stator teeth facing the inner and outer air gaps. Moreover, the axial force produced by the two rotors on the stator can be counteracted, which makes the stator support more reliable. Instead, for the counterpart with radial flux topology, the stator will suffer unbalanced radial force exerted by the two rotors.

Different with regular PM machines, the slots and teeth of the stator for VPM machine are not only for embedding windings or serving as part of the magnetic path, but also working as flux modulators, which has significant influence on torque performance of VPM machines. In order to maintain the same modulation effect along radial direction of an AFVPM machine, trapezoidal slot is desirable since the ratio of slot opening width to slot pitch remains constant. However, due to manufacturing difficulties, a radially proportional structure for an axial flux machine may not be a cost-effective option when silicon steel sheet are used to fabricate iron cores. Therefore, rectangular instead of trapezoidal slots are chosen for the proposed machine. On the rotor side, trapezoidal shaped magnets are preferred to keep the pole arc unchanged and thus remain a balanced magnetic loading along radial direction. Fig. 3 gives the sketch of the proposed machine, in which some main geometric parameters are tabulated in Table I.

TABLE I  
LIST OF MAIN GEOMETRIC PARAMETERS

Symbol	Meaning	Symbol	Meaning
$h_{ss}$	stator slot depth	$w_s$	stator slot width
$h_{ys}$	stator yoke thickness	$w_p(r)$	stator slot pitch
$h_{yr}$	rotor yoke thickness	$\theta_s$	stator mechanical angle
$h_m$	PM thickness	$\alpha_p$	PM pole arc coefficient
$g$	airgap length	$R_i$	machine inner radius
$L_l$	machine axial length	$R_o$	machine outer radius

## III. ANALYTICAL DERIVATION OF AXIAL FLUX VPM MACHINES

Since the proposed machine exhibits the property of mirror symmetry from the viewpoint of flux distribution, the derivation will be focused on half the whole model. That is to say, the following analyzing process is also applicable for regular AFVPM machine with only one surface mounted rotor and one single-side slotted stator. It should be noted that the reluctance as well as saturation of the steel parts is not considered. Besides, the radial component of flux is assumed to be negligible both in the airgap and steel region.

### A. Airgap Flux Density Excited by Magnets

According to the magnetic circuit theory in PM machines, one piece of PM can be regarded as one constant magnetomotive force (MMF) in series with a reluctance. With the choice of origin for  $\theta_s$  illustrated in Fig. 3 at the initial time, the Fourier series of the MMF  $F_c$  developed by PMs can be expressed by (1), where  $F_{c1}$  is the amplitude of the fundamental term,  $P_r$  the number of PM pole pairs,  $\omega$  the electrical angular velocity and  $\alpha_p$  the ratio of pole arc to pole pitch.  $F_{c1}$  is given by (2), where  $B_r$  and  $h_m$  are the remanence and thickness of the PM, respectively. With only the major term of  $F_c$  that

contributes to average torque production concerned, the components with higher order than  $i=1$  will be neglected in the following analysis.

$$F_c(\theta_s, t) = \sum_{i=1,3,5,\dots} \frac{F_{c1}}{i} \sin(i\alpha_p \frac{\pi}{2}) \cos(iP_r\theta_s - i\omega t) \quad (1)$$

$$\approx F_{c1} \cos(P_r\theta_s - \omega t)$$

$$F_{c1} = \frac{4}{\pi} \frac{B_r}{\mu_0\mu_r} h_m \sin(\frac{\pi}{2}\alpha_p) \quad (2)$$

The modulation effect of stator tooth-slot structure on the airgap flux density is an important aspect that differs VPM machines from regular PM machines. This effect should be represented by introducing the so-called airgap permeance function (3), rather than only the Carter factor. In (3),  $Z$  is the number of stator slots, while  $A_0$  and  $A_1$  stand for constant and fundamental term of the airgap permeance per unit area, respectively. The coefficients of the airgap permeance function can be further expressed by using the conformal mapping method in (4)~(7) [18], where  $\mu_0$  is the permeability of vacuum and  $\mu_r$  the relative permeability of PMs.  $w_s$ ,  $w_p(r)$  and  $g$  are the geometric parameters that have been described and summarized in Fig. 3 and Table I. Since  $w_s$  is constant for rectangular slots, the term  $w_s/w_p(r)$  becomes dependent on the radial position  $r$  and so does the airgap permeance function, which results in a varying flux modulation effect from the inner part to the outer part of the proposed machine.

$$A(\theta_s, r) \approx A_0(r) + A_1(r) \cos(Z\theta_s) \quad (3)$$

$$A_0(r) = \frac{\mu_0}{g'} [1 - 1.6\beta \frac{w_s}{w_p(r)}] \quad (4)$$

$$A_1(r) = \frac{\mu_0}{g'} \frac{2}{\pi} \beta \left\{ \frac{0.78125}{0.78125 - 2[\frac{w_s}{w_p(r)}]^2} \right\} \sin[1.6\pi \frac{w_s}{w_p(r)}] \quad (5)$$

$$g' = g + \frac{h_m}{\mu_r} \quad (6)$$

$$\beta = \frac{1}{2} \left\{ 1 - \left[ 1 + \left( \frac{w_s}{2g} \right)^2 \right]^{-\frac{1}{2}} \right\} \quad (7)$$

In order to exhibit the characteristics of  $A_0$  and  $A_1$ , a specific model of AFVPM machine has been built, whose major fixed parameters are listed in Table II. Fig. 4 and Fig. 5 give the variation of  $A_0$  and  $A_1$  with slot opening ratio (defined as  $w_s/w_p(r)$  calculated at average radius) and relative radial position, respectively. One should notice that  $w_s$  cannot exceed the minimum slot pitch  $w_{p-min}$ , (i.e.,  $w_p$  at innermost radius). It can be seen in Fig. 4 that  $A_0$  drops with the increase of slot opening ratio while remains almost unchanged along radial direction. Meanwhile, the situation for  $A_1$  is more complicated as shown in Fig. 5. At the inner part of the machine where  $2r/D_0$  is small,  $A_1$  decreases after an initial increase and reaches its peak value at the  $w_s/w_{p-avg}$  of around 0.55. However, this tendency

gradually disappears with the increase of radius  $r$ , which can be attributed to the limitation of  $w_s$  since the range of  $w_s/w_p$  keeps decreasing along radial direction and cannot reach an optimal value at the outer part of the machine. Since the airgap permeance function as well as flux modulation effect is changing along radial direction, the usual approximation for AFPM machines, i.e., equalizing them to corresponding linear machines by taking a 2D plane at the average radius, may result in larger errors for AFVPM machines than for regular AFPM machines.

TABLE II  
LIST OF MAIN MAJOR FIXED PARAMETERS

Symbol	Meaning	Quantity
$D_o$	stator outer diameter	220mm
$D_i$	stator inner diameter	132mm
$h_m$	PM thickness	3mm
$g$	airgap length	1mm
$B_r$	PM remanence	1.20T
$\alpha_p$	PM pole arc coefficient	0.9
$Z$	stator slot number	24
$P_r$	Rotor pole pair number	22

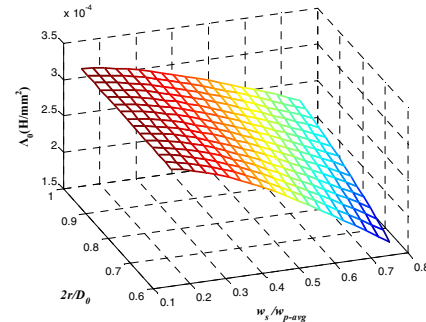


Fig. 4.  $A_0$  vs slot opening ratio  $w_s/w_{p-avg}$  & relative radial position  $2r/D_0$ .

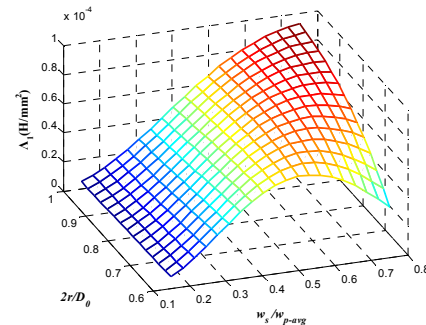


Fig. 5.  $A_1$  vs slot opening ratio  $w_s/w_{p-avg}$  & relative radial position  $2r/D_0$ .

$$B_g(\theta_s, r, t) = F_c(\theta_s, t) A(\theta_s, r) \quad (8)$$

$$B_g(\theta_s, r, t) \approx F_{c1} \left\{ A_0(r) \cos(P_r\theta_s - \omega t) + \frac{A_1(r)}{2} \cos[(Z - P_r)\theta_s + \omega t] + \frac{A_1(r)}{2} \cos[(Z + P_r)\theta_s - \omega t] \right\} \quad (9)$$

As illustrated in [9], the airgap flux density  $B_g$  is the production of PMs' MMF and the airgap permeance per unit

area, which yields (8). By substituting (1)~(3) into (8),  $B_g$  can be represented by (9), which is similar with that in [10]. However, it should be noticed that  $B_g$  is also related to radial position of the evaluated point, which is different from that for radial flux VPM machines.

### B. Back-EMF and Torque Expression

The winding function theory is applied to expediently derive the back-EMF and torque expression. For the proposed AFVPM machine with toroidal winding configuration, the flux linkage per phase  $\lambda_{ph}$  can be calculated by (10), where  $k$  is the diameter ratio (ratio of inner to outer diameter).  $N(\theta_s)$  is the winding function of one phase expressed by (11), where  $P_s$  is the number of stator pole pairs. Moreover, in VPM machines, the stator slot number and the pole pair number of the rotor and stator should satisfy the relationship expressed by (12).

$$\lambda_{ph} = \int_{kD_0/2}^{D_0/2} \int_0^{2\pi} B_g(\theta_s, r, t) N(\theta_s) d\theta_s ] r dr \quad (10)$$

$$N(\theta_s) = \sum_{j=1,3,5,\dots} \frac{2}{j\pi} \frac{N_s}{P_s} k_{wj} \cos(jP_s\theta_s) \quad (11)$$

$$P_s = |Z - P_r| \quad (12)$$

By substituting (9), (11) and (12) into (10),  $\lambda_{ph}$  can be represented by (13)~(15), where  $k_{wj}$  is the winding factor of  $j$ th harmonic,  $N_s$  the number of turns in series per phase. The plus and minus sign in (13) correspond to  $P_s=Z-P_r$  and  $P_s=Z+P_r$ , respectively. In the following analysis,  $P_s=Z-P_r$  is chosen for better torque performance of the proposed machine.

$$\lambda_{ph} = 2F_{c1}k_w \frac{N_s}{P_r} \cos \omega t (f_{A_0} \pm f_{A_1}) \quad (13)$$

$$f_{A_0} = \int_{kD_0/2}^{D_0/2} A_0(r) r dr = \frac{\mu_0}{8g} D_0^2 (1-k^2) \left(1 - \frac{1.6\beta w_s}{w_{p-avg}}\right) \quad (14)$$

$$f_{A_1} = \frac{P_r}{P_s} \int_{kD_0/2}^{D_0/2} \frac{1}{2} A_1(r) r dr \quad (15)$$

The back-EMF expression can then be obtained by (16), where  $\Omega$  stands for the rotor mechanical angular speed. For the proposed three-phase, surface-mounted AFVPM machine with negligible reluctance torque, the instantaneous electromagnetic torque  $T_e$  can be expressed by (17). Since the attention of this paper is focused on steady-state performance of the proposed machine from the viewpoint of electromagnetic field, the input current waveform is assumed to be sinusoidal. Therefore,  $T_e$  is further expressed by (18), where  $I_{ph}$  is the amplitude of phase current. As average electrical loading  $A_{avg}$  is given by (19),  $T_e$  can be replaced by (20).

$$e_{ph}(t) = -\frac{d}{dt} \lambda_{ph} = 2k_w N_s \Omega F_{c1} (f_{A_0} + f_{A_1}) \sin \omega t = E_{ph} \sin \omega t \quad (16)$$

$$T_e = \frac{e_a(t)i_a(t) + e_b(t)i_b(t) + e_c(t)i_c(t)}{\Omega} \quad (17)$$

$$T_e = \frac{3}{2} \frac{E_{ph} I_{ph}}{\Omega} = 3k_w F_{c1} N_s I_{ph} (f_{A_0} + f_{A_1}) \quad (18)$$

$$A_{avg} = \frac{3N_s I_{ph}}{\sqrt{2}\pi D_{avg}} = \frac{3\sqrt{2}N_s I_{ph}}{\pi(1+k)D_0} \quad (19)$$

$$T_e = \frac{\sqrt{2}\pi}{2} k_w F_{c1} A_{avg} (1+k) D_0 (f_{A_0} + f_{A_1}) \quad (20)$$

It can be seen from (16) and (18) that both the back-EMF and torque are proportional to the term  $f_{A_0} + f_{A_1}$ , which is decided by the main geometric parameters of the proposed machine.  $f_{A_0}$  is directly expressed with these parameters in (12) and  $f_{A_1}$  in (13) can be evaluated by numerical integration. Essentially,  $f_{A_0}$  and  $f_{A_1}$  are proportional to constant and fundamental term of the real permeance over the entire airgap region. Analogous to the analytical equations for radial flux VPM machines [9],  $f_{A_0}$  can be regarded as the coefficient for a conventional AFPM machine, while  $f_{A_1}$  is the additional term brought in by the vernier structure. It is easily seen that the parameters affecting  $f_{A_0}$  and  $f_{A_1}$  are  $D_0$ ,  $k$ ,  $w_s$ ,  $g$ ,  $P_r$  and  $P_s$ . By now, the influence of these parameters on output torque of the proposed AFVPM machine can be investigated analytically.

Since  $f_{A_0} + f_{A_1}$  is proportional to the torque production, the relationship of some key design parameters with it is analyzed. Fig. 6 gives the variation of  $f_{A_0}$  and  $f_{A_1}$  with slot opening ratio for different diameter ratios. It can be seen that  $f_{A_1}$  exceeds corresponding  $f_{A_0}$  as  $w_s/w_{p-avg}$  gets larger than 0.45. That is to say, the torque capability of an AFVPM machine can be more than twice that of its conventional counterpart. The variation of  $f_{A_0} + f_{A_1}$  with slot opening ratio at different diameter ratios is illustrated in Fig. 7. It can be seen that  $f_{A_0} + f_{A_1}$  drops along with the increase of  $k$ , while the optimal values of  $w_s/w_{p-avg}$  share a common number of around 0.6 for the pole ratio of 22/2. The relationship of  $f_{A_0} + f_{A_1}$  with slot opening ratio for different pole ratios is shown in Fig. 8, from which it can be seen that the optimal values of  $w_s/w_{p-avg}$  increases when the pole ratio gets larger.

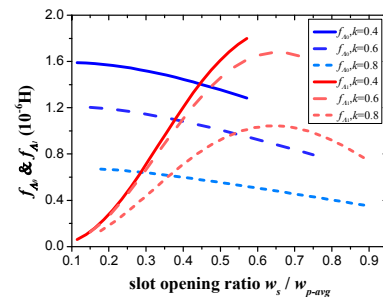


Fig. 6.  $f_{A_0}$  &  $f_{A_1}$  vs slot opening ratio  $w_s/w_{p-avg}$  with different diameter ratios.  $P_r=22$ ,  $P_s=2$ ,  $g=4$ mm.

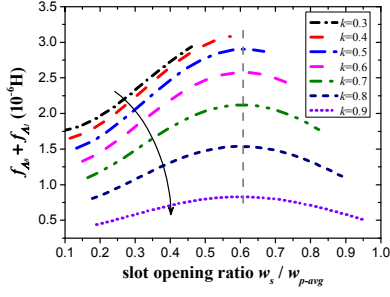


Fig. 7.  $f_{A_0} + f_{A_1}$  vs slot opening ratio  $w_s / w_{p-avg}$  with different diameter ratio.  $P_r = 22$ ,  $P_s = 2$ ,  $g = 4\text{mm}$ .

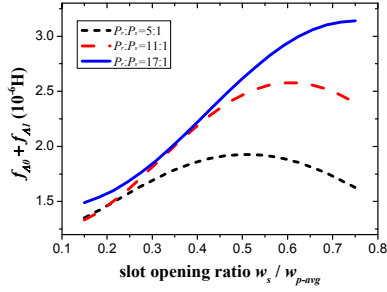


Fig. 8.  $f_{A_0} + f_{A_1}$  vs slot opening ratio  $w_s / w_{p-avg}$  with different pole ratio.  $P_s = 2$ ,  $g = 4\text{mm}$ .

During the torque analysis through the derived equations, some fixed parameters are listed in Table III. The DC copper loss is kept constant to fix the thermal condition, viz:

$$\begin{aligned} P_{Cu} &= ZP_{st} = ZN_s \left( \frac{I_{ph}}{\sqrt{2}C} \right)^2 r_{sl} \\ &= ZN_s^2 \frac{I_{ph}^2 \rho_{Cu} (1-k) D_0}{2C^2 2k_{Cu} A_s} \end{aligned} \quad (21)$$

where  $N_s$  is the number of conductors in a slot,  $C$  the number of parallel branches per phase,  $r_{sl}$  the resistance of the slot portion of each conductor,  $k_{Cu}$  the slot fill factor,  $\rho_{Cu}$  the resistivity of copper and  $A_s$  the area of each slot.

Since  $I_{ph}$  is held constant, the number of turns in series per phase should be limited by (22).

$$N_s \propto \sqrt{\frac{A_s}{(P_r + P_s)(1-k)D_0}} \quad (22)$$

TABLE III  
LIST OF FIXED PARAMETERS FOR TORQUE ANALYSIS

Symbol	Meaning	Quantity
$D_o$	stator outer diameter	220mm
$h_m$	PM thickness	3mm
$g$	airgap length	1mm
$B_r$	PM remanence	1.20T
$\alpha_p$	PM pole arc coefficient	0.9
$I_{ph}$	peak phase current	16.7A
$P_{Cu}$	DC copper loss	80W

The diameter ratio  $k$  is a key parameter for AFPM machines. The tendency shown in Fig. 7 does not mean that the diameter

ratio should be as small as possible, since it does not take the copper loss into account. The pole ratio, defined as the ratio of rotor to stator pole pair number, is an important design parameter for VPM machines, which must be carefully chosen. Therefore, the influence of  $k$  and pole ratio on the torque performance is investigated through the analytical torque equation. Fig. 9 and Fig. 10 give the torque variation with  $k$  for different combinations of  $P_s$  and  $P_r$ . It can be seen from Fig. 9 that the proposed machines with higher pole ratio and the same stator pole pair number may achieve larger average torque. Fig. 10 shows the torque variation with  $k$  when the pole ratio is fixed at 11/1. It can be seen that the lower stator pole pair number leads to larger torque and the optimal  $k$  for the pole ratio of 11/1 is around 0.6.

The airgap structures, such as slot opening ratio, magnet thickness, airgap length etc., also have significant influence on torque performance of the proposed machine. The effects of these parameters will be investigated through the derived equations in association with FEA in section IV.

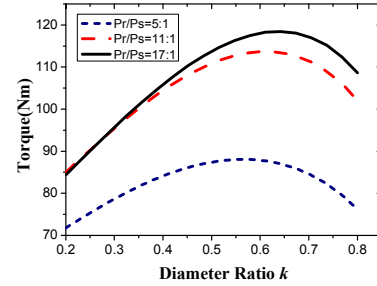


Fig. 9. Torque vs  $k$  with different pole ratio.  $P_s = 2$ ,  $w_s / w_{p-avg} = 0.5$

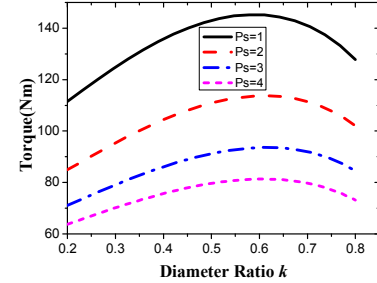


Fig. 10. Torque vs  $k$  with different stator pole pair number. Pole ratio=11/1.  $w_s / w_{p-avg} = 0.5$ .

#### IV. VERIFICATION OF ANALYTICAL METHOD WITH QUASI-3D FEA AND 3D FEA

##### A. Verification by Quasi-3D FEA

As axial flux machines have inherent 3D flux path, the most accurate solution to verify the proposed equations is to apply 3D FEA. However, the simulation of 3D FEA models will be too time-consuming when the design parameters are changing. Therefore, the so-called quasi-3D FEA is employed to make more efficient comparison with the analytical results. As illustrated in Fig. 11, the real 3D model is “cut” into several layers along concentric cylindrical surfaces at certain radius, with each segment being “straightened” to a rectangular model. These rectangular models can be regarded as linear machines

and analyzed with 2D FEA. The overall performance of the whole machine can then be obtained by summing the performance of all the layers. Essentially, this method is a multi-layer 2D FEA. In this part, the layer number are chosen as five to balance the computation time and accuracy. By adopting the quasi-3D FEA instead of conventional 2D FEA, the variation of structural parameters along radial direction is simplified but still taken into account, which makes the comparison more convincing.

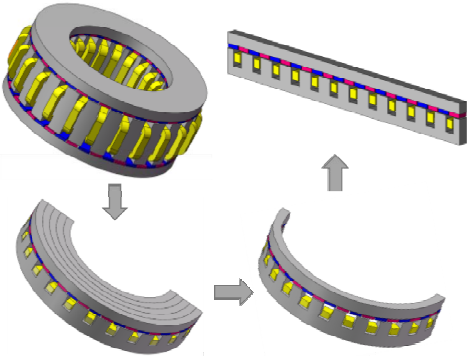


Fig. 11. Schematic of transforming the 3D model of the proposed machine to corresponding quasi-3D model.

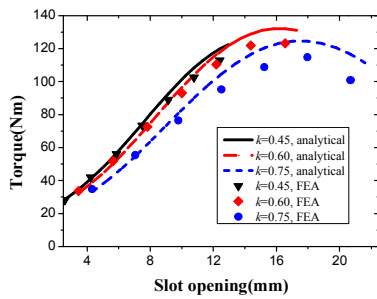


Fig. 12. Torque vs slot opening with different diameter ratio  $k$ .  $g=1\text{mm}$ .

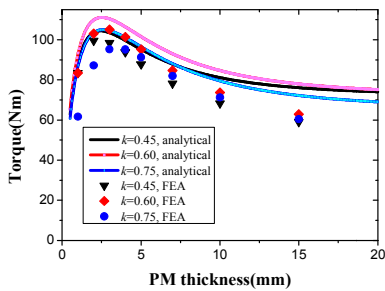


Fig. 13. Torque vs PM thickness with different diameter ratio  $k$ .  $g=1\text{mm}$ .

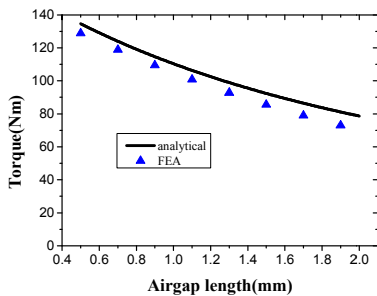


Fig. 14. Torque vs airgap length. Diameter ratio  $k=0.6$ .

To verify the derived equations, several quasi-3D FEA models have been built. Fig. 12 gives the comparison of torque variation with slot opening between analytical method and FEA. It can be seen that the results match well. Moreover, it should be noted that for AFPM machines, the range of values for slot opening is dependent on the diameter ratio. The larger the diameter ratio is, the wider the range of values for slot opening will be. For  $k=0.6$ , the optimal slot opening ratio is  $\sim 0.63$ . In practical case, the selection of slot opening and diameter ratio should also take into account the room for end winding and tooth saturation at the inner part of the machine.

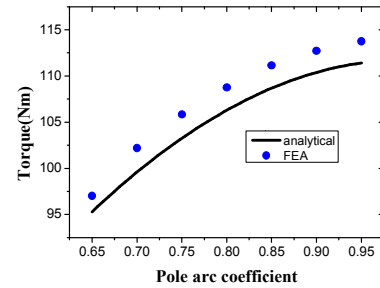


Fig. 15. Torque vs pole arc coefficient  $\alpha_p$ . Diameter ratio  $k=0.6$ .

Fig. 13 shows the torque variation with PM thickness for different values of  $k$ . In each curve, the torque increases rapidly and reaches its peak value at the PM thickness of around 2.6mm and drops slowly ever since. The gap between analytical results and FEA gets larger since PM thickness exceeds 10mm, which can be attributed to considerable flux leakage between adjacent magnets. The variations of torque with airgap length and pole arc coefficient are illustrated and compared in Fig. 14 and Fig. 15, respectively, in which the results coincide well. Overall, sufficient accuracy has been verified within a wide variation range of corresponding parameters.

### B. Verification by 3D FEA

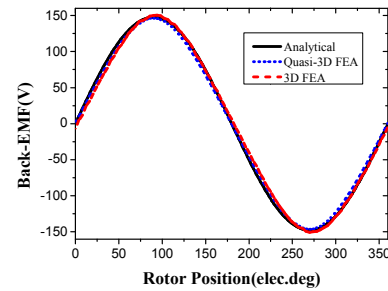


Fig. 16. Comparison of back-EMF waveforms.

In order to validate both the theoretical and quasi-3D FEA results, a 3D FEA model has been built, whose geometric parameters have been optimized based on the foregoing analysis. The major machine parameters are listed in Table IV, in which the electrical loading is calculated at the average radius. It should be reminded that only the fundamental term of back-EMF and torque is considered in theoretical analysis. Fig.

16 illustrates the comparison of back-EMF waveforms between the analytical, quasi-3D FEA and 3D FEA results. It can be seen that the waveforms match well with each other. Fig. 17 gives the comparison of torque waveforms, in which the analytical value is 110.3Nm, ~4% larger than the average torque from 3D FEA. With the current density of 4.2 A/mm<sup>2</sup>, the torque density of the 3D model can reach 32.6 kNm/m<sup>3</sup>. The torque ripples of the quasi-3D model and 3D model are 0.5% and 2.3%, respectively. The comparison of the three methods is summarized in Table V.

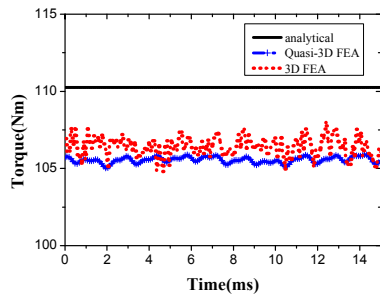


Fig. 17. Comparison of torque waveforms.

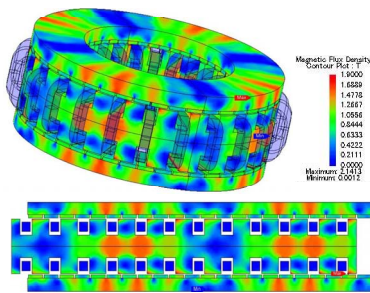


Fig. 18 Magnetic field plot of the 3D FEA model and the outermost layer of quasi-3D FEA model.

The magnetic field plot of the 3D model and the outermost layer of quasi-3D model is shown in Fig. 18. It can be seen that the flux density distribution of the two models coincide well and the peak value is around 1.65T in both the stator and rotor yoke.

TABLE IV  
Main Design Parameters of the Machine

Item	Value
Number of slots	24
Number of rotor pole pair	22
Stator outer diameter	220mm
Diameter ratio	0.6
Axial length	91mm
Magnet thickness	3.0mm
Airgap length	1.0mm
Slot depth	12.0mm
Slot width	11.5mm
Slot opening ratio	0.5
Electrical loading	164A/cm
Current density	4.2A/mm <sup>2</sup>
Turns in series per phase	256
Rotation speed	320rpm
Pole arc coefficient	0.9
Temperature	100°C

TABLE V  
COMPARISON OF THE THREE METHODS

Item	Analytical	Quasi-3D	3D
Avg. Torque /Nm	110.3	105.6	106.1
Torque density /kNm/m <sup>3</sup>	33.9	32.7	32.6
Torque ripple	-	0.5%	2.3%
Calculation time	<1s	40min	8hour

## V. PROTOTYPE AND AUXILIARY MECHANICAL STRUCTURE

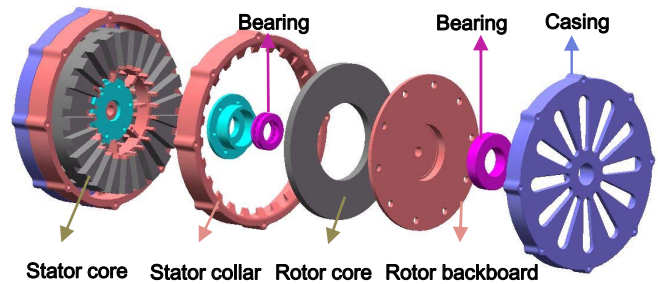


Fig. 19. Exploded view of mechanical structure of the proposed AFVPM prototype. The windings and PMs are hid.



Fig. 20. Stator and rotor iron cores of the prototype.

In order to validate the foregoing analysis, a dual-rotor, toroidal-winding AFVPM prototype machine has been designed and still being manufactured, whose main design parameters are exactly based on the 3D model in Section IV and listed in Table IV. Fig. 19 illustrates the exploded sketch of the prototype and auxiliary mechanical structure, in which the windings and PMs are hid. Due to the toroidal winding configuration, the support for the intermediate stator should be designed specifically. In addition, turntable bearing is used to counteract the large axial force exerted on the rotor. The stator and rotor iron cores, fabricated with rolling silicon steel sheet, is shown in Fig. 20. The test of the prototype will be conducted to testify the superiority of the proposed machine as well as complete the validation of the forgoing analysis.

## VI. CONCLUSION

In this paper, a dual-rotor, toroidal-winding, axial flux vernier permanent magnet (AFVPM) machine has been proposed. Benefited from the rotor-stator-rotor topology combined with the North-North (N-N) type magnet polarity arrangement, the overall end winding length is significantly reduced by the adoption of toroidal winding. In order to investigate the nature of AFVPM machines, the back-EMF and

torque equations of an AFVPM machine have been derived using the airgap permeance function. The influence of parameters, such as pole ratio, diameter ratio, slot opening, PM thickness and airgap length on torque performance has been investigated based on the proposed equations.

The so-called quasi-3D FEA has been employed to verify the proposed equations. Comparison has been made between torque values from the FEA and analytical equations within a wide range of design parameters and the results turn out to match well.

A real 3D FEA of the proposed machine has been conducted to compare with the forgoing theoretical and quasi-3D FEA results. The back-EMF and torque waveforms coincide well. Therefore, sufficient accuracy of the proposed analytical equations has been verified. Finally, a corresponding prototype machine has been designed and under manufacturing process. Experimental validation will be conducted in the future.

## VII. ACKNOWLEDGEMENT

This work was supported by two grants from National Natural Science Foundation of China (NSFC) under Project No. 51337004 and Project No. 51407082.

## REFERENCES

- [1] A. Toba and T. Lipo, "Generic torque-maximizing design methodology of surface permanent-magnet vernier machine," *IEEE Trans. Ind. Appl.*, vol. 36, no. 6, pp. 2032-2035, Jun.2005.
- [2] D. Li, R. Qu, and Z. Zhu, "Comparison of Halbach and dual-side vernier permanent magnet machines," *IEEE Trans. Magn.*, vol. 50, no. 2, pp. 7019804, Feb. 2014.
- [3] S. Niu, S. Ho, W. Fu, and L. Wang, "Quantitative comparison of novel vernier permanent magnet machines," *IEEE Trans. Magn.*, vol. 46, no. 6, pp. 2032-2035, June. 2005.
- [4] R. Qu, D. Li, and J. Wang, "Relationship between magnetic gears and vernier PM machines," in *Proc. Int. Conf. Electrical Machines & Systems*, Beijing, China, Aug. 18–20, 2011, pp:1-6.
- [5] D. Li, R. Qu, and T. Lipo, "High power factor vernier permanent magnet machines," *IEEE Trans. Ind. Appl.*, vol. 50, no. 6, pp. 3664-3674, Nov./Dec. 2014.
- [6] D. Li, R. Qu, J. Li, and W. Xu, "Design of consequent pole, toroidal winding, outer rotor vernier permanent magnet machines," in *Proc. 2014 IEEE Ener. Con. Cong. & Exp.*, Sep. 2014, pp.2342 - 2349.
- [7] S. Niu, S. L. Ho, W. N. Fu, and L. L. Wang, "Quantitative comparison of novel vernier permanent magnet machines," *IEEE Trans. Magn.*, vol. 46, no. 6, pp. 2032–2035, Jun. 2005.
- [8] J. Li, K. T. Chau, J. Jiang, C. Liu and W. Li, "A new efficient permanent-magnet vernier machine for wind power generation," *IEEE Trans. Magn.*, vol. 46, no. 6, pp.1475-1478, Jun. 2010.
- [9] B. Kim, and T. Lipo, "Operation and design principles of a PM vernier motor," *IEEE Trans. Ind. Appl.*, vol. 50, no. 6, pp. 3656-3663, Nov./Dec. 2014.
- [10] D. Li, R. Qu, J. Li, L. Wu, and W. Xu, "Analysis of torque capability and quality in vernier permanent magnet machines," in *Proc. Int. Conf. Electrical Machines and Systems*, Oct. 2014, pp.3620-3626.
- [11] A. Cavagnino, M. Lazzari and F. Profumo, "A comparison between the axial flux and the radial flux structures for PM synchronous motors," *IEEE Trans. Ind. Appl.*, vol. 38, no. 6, pp. 1517-1524, Nov./Dec. 2002.
- [12] S. Huang, J. Luo, F. Leonardi, and T. Lipo, "A comparison of power density for axial flux machines based on general purpose sizing equations," *IEEE Trans. Energ. Convers.*, vol. 14, no. 2, pp. 185-192, Jun. 1999.
- [13] A. Egea, G. Almandoz, J. Poza, G. Ugalde, and A. J. Escalada, "Axial-flux-machine modeling with the combination of FEM-2-D and analytical tools," *IEEE Trans. Ind. Appl.*, vol. 48, no. 4, pp. 1318-1326, July./Aug. 2012.
- [14] A. Parviainen, M. Niemelä, and J. Pyrhönen, "Modeling of axial flux permanent-magnet machines", *IEEE Trans. Ind. Appl.*, vol. 3640, no. 5, pp. 1333-1340, Sep./Oct. 2004.
- [15] F. Zhao, T. Lipo, B. Kwon, "A novel dual-stator axial-flux spoke-type permanent magnet Vernier machine for direct-drive applications," *IEEE Trans. Magn.*, vol. 50, no. 11, pp. 8104304, Nov. 2014.
- [16] L. Li, W. N. Fu, S. Niu and Y. Li, "A quantitative comparison study of power electronic driven flux-modulated machines using magnetic field and thermal field co-simulation", *IEEE Trans. Ind. Electron.*, in press.
- [17] T. Zou, R. Qu, J. Li, and D. Li, "A consequent pole, dual rotor, axial flux vernier permanent magnet machine", *Int. Conf. Ecological Vehicles and Renewable Energies*, Monte Carlo, Monaco, Mar. 31–Apr. 2, 2015, pp:1-9.
- [18] Z. Q. Zhu and D. Howe, "Instantaneous magnetic-field distribution in brushless permanent-magnet dc motors, part III effect of stator slotting," *IEEE Trans. Magn.*, vol. 29, no. 1, pp. 143-151, Jan. 1993.